




Non-classical photonic spin texture of quantum structured light

Li-Ping Yang ^{1,2} & Zubin Jacob ² 

Classical structured light with controlled polarization and orbital angular momentum (OAM) of electromagnetic waves has varied applications in optical trapping, bio-sensing, optical communications and quantum simulations. However, quantum noise and photon statistics of three-dimensional photonic angular momentum are relatively less explored. Here, we develop a quantum framework and put forth the concept of quantum structured light for space-time wavepackets at the single-photon level. Our work deals with three-dimensional angular momentum observables for twisted quantum pulses beyond scalar-field theory as well as the paraxial approximation. We show that the spin density generates modulated helical texture and exhibits distinct photon statistics for Fock-state vs. coherent-state twisted pulses. We introduce the quantum correlator of photon spin density to characterize nonlocal spin noise providing a rigorous parallel with electronic spin noise. Our work can lead to quantum spin-OAM physics in twisted single-photon pulses and opens explorations for phases of light with long-range spin order.

¹Center for Quantum Sciences and School of Physics, Northeast Normal University, Changchun, China. ²Birck Nanotechnology Center, School of Electrical and Computer Engineering, Purdue University, West Lafayette, IN, USA. ✉email: zjacob@purdue.edu

Structured single-photon pulses are an important frontier for spin and orbital angular momentum (OAM)^{1–3}. As a quantum information carrier, single-photon pulses with OAM have been achieved in the solid-state system with quantum dots recently⁴ and have been exploited to construct a quantum network with higher channel capacity^{5–10}. The spin and OAM of light have also attracted increasing attention in an emerging research field—spin-orbit photonics¹¹, which studies photon spin-OAM transfer^{12–15} and light–matter angular momentum exchange in the near-field region^{16–18} or transfer of optical OAM to bounded electrons¹⁹ or photoelectrons^{12,20}. Spin-1 quantization is also the hallmark of photonic skyrmions and topological photonic phases of matter^{21,22}. A quantum field theory framework is needed to study the non-classical properties such as 3D noise of the angular momentum of light.

Existing theories of quantum light–matter interaction have advanced over the last two decades to capture a plethora of phenomena related to SAM and OAM of light^{23–34}. Important outstanding questions remain even within this large body of work which is the focus of this manuscript, namely—photon statistics, 3D quantum spin and OAM vector density, 3D quantum noise in SAM/OAM, and single-photon quantum states. Figure 1a shows the well-known regime of twisted laser beams which contain an enormous number of photons. At the single-photon level, both existing semi-classical^{23,24} and approximate quantum theories break down^{30,32}. In the widely adopted state-space description of single photons or entangled photons $\{|l, s\rangle\}$ with Stokes parameters and the Poincaré sphere^{28,33}, the rich spatial texture of spin and OAM vectors is ignored completely. Specifically, important open questions remain on the full 3D projection of photon spin and OAM at the quantum level beyond the scalar-field theory and paraxial approximation. Heisenberg uncertainty relations for photon angular momenta can affect quantum metrology experiments which require a quantum theoretic framework. These Heisenberg uncertainty relations between different photon OAM 3D components are the canonical quantum characteristics of angular momentum. Similarly, for applications such as secure quantum communication, twisted single-photon pulses in the quantum limit with few photons (see Fig. 1b) are required. In this technologically relevant limit, quantum statistics of photons will reveal behavior significantly different from the quasi-classical Poisson behavior exhibited by traditional OAM laser beams. These fundamental, as well as technologically relevant problems, require the definition of single-photon quantum state along with OAM/SAM operators.

In this work, we present an important frontier for quantum structured light involving twisted space–time wavepackets of light. We first construct the wave function of a quantum twisted pulse, as well as a twisted laser beam, from quantum field

theory³⁵ instead of from the single-particle Schrödinger equation in the first-quantization picture^{36–38}. By exploiting the quantum operators of the angular momenta of light³⁹, we evaluate the mean value, as well as the quantum uncertainty of the photon spin operator vector. Apart from the well-established global properties of polarization, we also investigate the quantum properties of the photon spin density vector, i.e., the spin texture, which is a function of space and time. We show that beyond the paraxial approximation, the photon spin density of a Bessel single-photon pulse can exhibit rich spatial texture. Our work builds on previous important work in the field^{23–34}. Our proposed framework provides a powerful and versatile tool to engineer the local photon spin and OAM densities of a quantum structured light pulse, specifically for spatiotemporal optical vortices^{40,41}.

Non-local spin noise (i.e., spin density correlation) for electrons is a fundamental signature of quantum phases of magnetic condensed matter⁴², specifically in phases of matter such as quantum spin liquids without magnetic order⁴³. However, no such quantum spin noise operator has been defined for photons till date. Our theoretical formalism allows us to overcome this challenge. Here, we introduce the quantum correlator of photonic spin density to characterize the nonlocal spin noise in light. This paves the way to explore exotic phases of light with long-range spin order.

We emphasize that our work is immediately amenable to experimental verification. We predict that for Bessel pulses with large OAM, there will exist large fluctuations in the OAM along orthogonal directions. This additional quantum noise can be verified in metrology experiments even with OAM laser beams. Recently, it was demonstrated that the nitrogen-vacancy (NV) center in diamond can be used as a quantum sensor for detecting the local spinning nature of photons⁴⁴. The spin density of the off-resonant optical beam can induce an effective static magnetic field for the electron spin of the NV center, which itself is an atomic-scale magnetometer working at room temperature. Imaging of our discovered helical spin-density structure in this work can be realized with the same technology in the near future. Furthermore, our proposed non-local spin density correlation can also be measured in compound measurements with two or multiple NV centers.

Results and discussion

Quantum spin and orbital angular momenta of light. The full quantum operator of photon spin is given by³⁹

$$\hat{S} = \frac{1}{c} \int d^3x \hat{\pi}(\mathbf{r}, t) \times \hat{A}(\mathbf{r}, t). \quad (1)$$

and OAM \hat{L} of light in the Lorenz gauge within quantum field

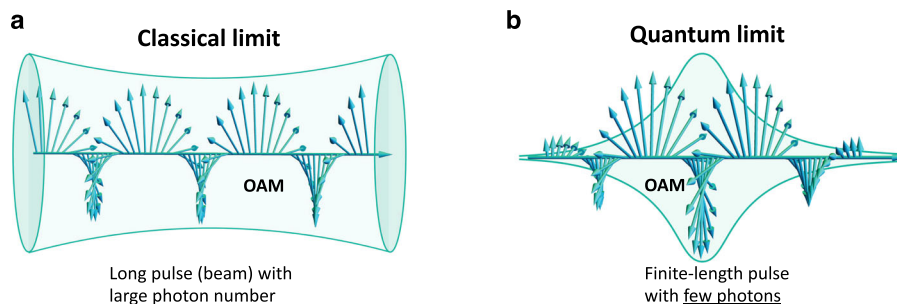


Fig. 1 Contrast between a traditional twisted beam and quantum pulse. Schematic of a traditional twisted beam **a** compared to the quantum twisted pulse **b** put forth in this paper. The semi-classical theory only captures the mean orbital angular momentum (OAM) of a laser beam with large photon number. However, the quantum effects of photon statistics, vectorial uncertainty relations, and non-local spin noise require a quantum-theoretical framework put forth in this paper.

theory. The operators $\hat{\mathbf{S}}$ and $\hat{\mathbf{L}}$ obey the canonical commutation relationships

$$[\hat{S}_i, \hat{S}_j] = i\hbar\epsilon_{ijk}\hat{S}_k, [\hat{L}_i, \hat{L}_j] = i\hbar\epsilon_{ijk}\hat{L}_k, [\hat{L}_i, \hat{S}_j] = 0, \quad (2)$$

where ϵ_{ijk} is the third-order Levi-Civita symbol. The longitudinal and scalar photons play a significant role in both $\hat{\mathbf{S}}$ and $\hat{\mathbf{L}}$. However, only the SAM $\hat{\mathbf{S}}^{\text{obs}} = \epsilon_0 \int d^3r \hat{\mathbf{E}}_{\perp}(\mathbf{r}, t) \times \hat{\mathbf{A}}_{\perp}(\mathbf{r}, t)$ and OAM $\hat{\mathbf{L}}^{\text{obs}} = \epsilon_0 \int d^3r \hat{\mathbf{E}}_{\perp}^j(\mathbf{r}, t)(\mathbf{r} \times \nabla) \hat{\mathbf{A}}_{\perp}^j(\mathbf{r}, t)$ carried by transversely polarized photons are directly observable quantities even in the presence of charges³⁹. Note, $\hat{\mathbf{E}}_{\perp}$ and $\hat{\mathbf{A}}_{\perp}$ are the transverse part of the electric field and the vector potential, respectively.

Using the circularly polarized plane waves, we can expand the observable photon spin and OAM operators as^{45–47} (please refer to Supplementary Notes 1 and 2)

$$\hat{\mathbf{S}}^{\text{obs}} = \hbar \int d^3k \left[\hat{a}_{\mathbf{k},+}^{\dagger} \hat{a}_{\mathbf{k},+} - \hat{a}_{\mathbf{k},-}^{\dagger} \hat{a}_{\mathbf{k},-} \right] \mathbf{e}(\mathbf{k}, 3), \quad (3)$$

$$\hat{\mathbf{L}}^{\text{obs}} = -i\hbar \int d^3k \sum_{\lambda=\pm} \hat{a}_{\mathbf{k},\lambda}^{\dagger} (\mathbf{k} \times \nabla_{\mathbf{k}}) \hat{a}_{\mathbf{k},\lambda}, \quad (4)$$

where $\mathbf{e}(\mathbf{k}, 3) = \mathbf{k}/|\mathbf{k}|$ is the unit vector and $\lambda = \pm$ denotes the left circular polarization (LCP) and right circular polarization (RCP) separately (see Supplementary Note 1). The ladder operators of the plane wave with wave vector \mathbf{k} and polarization λ satisfy the bosonic commutation relation $[\hat{a}_{\mathbf{k},\lambda}, \hat{a}_{\mathbf{k}',\lambda'}^{\dagger}] = \delta(\mathbf{k} - \mathbf{k}')\delta_{\lambda\lambda'}$. The photon helicity is given by $\hat{\Lambda} = \hbar \int d^3k \left[\hat{a}_{\mathbf{k},+}^{\dagger} \hat{a}_{\mathbf{k},+} - \hat{a}_{\mathbf{k},-}^{\dagger} \hat{a}_{\mathbf{k},-} \right]$. We emphasize that the spin and OAM are separately observable due to the quantum commutation relations³⁹

$$[\hat{S}_i^{\text{obs}}, \hat{L}_j^{\text{obs}}] = 0. \quad (5)$$

To show the striking symmetry between the angular momentum of photons and electrons, we define a field operator for light in real space $\hat{\psi}(\mathbf{r}) = [\hat{\psi}_+(\mathbf{r}), \hat{\psi}_-(\mathbf{r})]^T$, where

$$\hat{\psi}_{\lambda}(\mathbf{r}) = \frac{1}{\sqrt{(2\pi)^3}} \int d^3k \hat{a}_{\mathbf{k},\lambda} e^{i\mathbf{k}\cdot\mathbf{r}}. \quad (6)$$

For the source-free case, our defined field operator in the Heisenberg picture satisfies the homogeneous wave equation

$$\left(\nabla^2 - \frac{1}{c^2} \frac{\partial^2}{\partial t^2} \right) \hat{\psi}(\mathbf{r}, t) = 0. \quad (7)$$

Now, we can re-express the OAM and helicity operators of light in parallel to their electron counterparts

$$\hat{\mathbf{L}}^{\text{obs}} = \int d^3r \hat{\psi}^{\dagger}(\mathbf{r})(\mathbf{r} \times \hat{\mathbf{p}})\hat{\psi}(\mathbf{r}), \quad (8)$$

and

$$\hat{\Lambda} = \hbar \int d^3r \hat{\psi}^{\dagger}(\mathbf{r})\hat{\sigma}_z\hat{\psi}(\mathbf{r}) \quad (9)$$

where $\hat{\mathbf{p}} = -i\hbar\nabla$ is momentum operator and $\hat{\sigma}_z = \text{diag}[1, -1]$ is the Pauli matrix. However, the similar expression for the spin operator $\hat{\mathbf{S}}^{\text{obs}}$ can not be obtained in real space. The unit polarization vector $\mathbf{e}(\mathbf{k}, 3)$ in Eq. (3) for each plane wave is \mathbf{k} -dependent, i.e., dependent on its spatial momentum.

Quantum wave function of twisted light pulses. In previous sections, we have shown that both $\hat{\mathbf{S}}^{\text{obs}}$ and $\hat{\mathbf{L}}^{\text{obs}}$ are vector operators. However, in previous studies, usually only their projections on the propagating direction have been fully studied^{23,24,34}. Their mean value on the transverse plane and more importantly, their quantum fluctuations have not been

investigated. On the other hand, the near-field techniques have now been well developed. This makes it possible to measure and engineer the angular-momentum density of light, which is a vector function of space and time, in experiments. Thus, a fully quantum theory beyond the paraxial approximation to explore all classes of twisted pulses in a united framework is highly desirable. Here, we present this powerful theoretical tool by generalizing the quantum theory of continuous-mode field^{35,48} to the twisted-pulse case.

We first define the single-photon wave-packet creation operator for a twisted photon pulse

$$\hat{a}_{\xi\lambda}^{\dagger} = \int d^3k \xi_{\lambda}(\mathbf{k}) \hat{a}_{\mathbf{k}\lambda}^{\dagger}, \quad (10)$$

as a coherent superposition of plane-wave modes. The pulse shape and other quantum properties of the pulse are fully determined by the spectral amplitude function (SAF) $\xi_{\lambda}(\mathbf{k})$. In the following, we denote the propagating direction of the pulse as the z -axis and work in the cylindrical coordinate in k -space $\mathbf{k} = k_z \mathbf{e}_z + \rho_k \mathbf{e}_{\rho} = \rho_k \cos \varphi_k \mathbf{e}_x + \rho_k \sin \varphi_k \mathbf{e}_y + k_z \mathbf{e}_z$. Here, ρ_k is the radial distance from the k_z -axis, φ_k is the azimuth angle, and \mathbf{e} denotes the corresponding unit vector. The SAF of a twisted pulse with deterministic OAM can be generally expressed as

$$\xi_{\lambda}(\mathbf{k}) = \frac{1}{\sqrt{2\pi}} \eta_{\lambda}(k_z, \rho_k) e^{im\varphi_k}. \quad (11)$$

Usually, the amplitude $\eta_{\lambda}(k_z, \rho_k)$ is symmetric in the transverse plane, i.e, it is independent on the azimuth angle φ_k . The phase factor $\exp(im\varphi_k)$ with an integer m will lead to the OAM of light in z -direction of a single-photon pulse as shown in the following.

The SAF is required to satisfy the normalization condition $\int d^3k |\xi_{\lambda}(\mathbf{k})|^2 = 1$. This guarantees that $\hat{a}_{\xi\lambda}^{\dagger}$ obey the bosonic commutation relation

$$[\hat{a}_{\xi\lambda}, \hat{a}_{\xi\lambda}^{\dagger}] = 1. \quad (12)$$

Then, the wave-packet creation operator $\hat{a}_{\xi\lambda}^{\dagger}$ can be treated as a normal ladder operator of a harmonic oscillator. Using this commutation relation, we can construct the wave function of all classes of quantum pulses in the standard way, such as the most common n -photon Fock-state and coherent-state pulses³⁵ (please refer to Supplementary Note 3)

$$|n_{\xi\lambda}\rangle = \frac{1}{\sqrt{n!}} (\hat{a}_{\xi\lambda}^{\dagger})^n |0\rangle, \quad (13)$$

and

$$|\alpha_{\xi\lambda}\rangle = \exp\left(\alpha \hat{a}_{\xi\lambda}^{\dagger} - \frac{1}{2}\bar{n}\right) |0\rangle = e^{-\bar{n}/2} \sum_{n=0}^{\infty} \frac{\alpha^n}{\sqrt{n!}} |n_{\xi\lambda}\rangle, \quad (14)$$

where $\bar{n} = |\alpha|^2$ is the mean photon number in the coherent-state pulse. The wave function of a squeezed-state pulse, an entangled two-photon pulse⁴⁹, or an ultra-short spatiotemporal vortex pulse^{40,41} can also be constructed similarly. Here, the polarization of the pulse is fixed as one of the circular polarizations. However, linearly or elliptically polarized quantum pulses can also be constructed with the superposition of two circular polarization ladder operators $\hat{a}_{\xi\lambda}$ ($\lambda = \pm$). We also note that a twisted laser beam can be characterized by a wave function with a very long pulse length and a very large photon number. Thus, our method also captures the cases of continuous OAM laser beams used widely in experiments.

Without loss of generality, we only take the Bessel pulses as an example to show the quantum properties of the spin and OAM of twisted pulses. Other twisted pulses, such as a Bessel–Gaussian or Laguerre–Gaussian pulse, can be treated similarly. The single-frequency Bessel beam is the superposition of all plane waves on

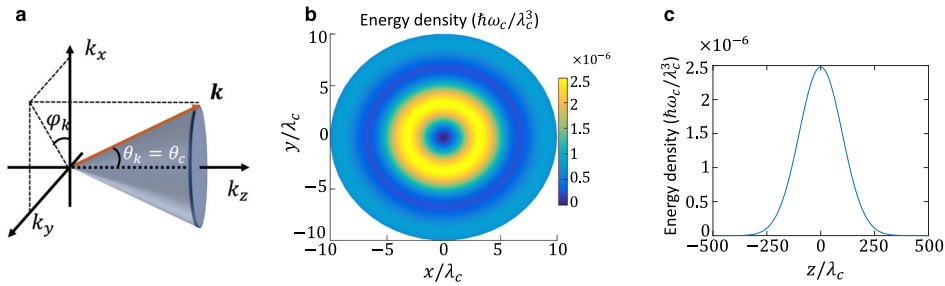


Fig. 2 Profile of a Bessel pulse in wave-vector space and real space. **a** Schematic of the spectral distribution of a Bessel pulse. **b** The energy density (in unit of $\hbar\omega_c/\lambda_c^3$) distribution of a Bessel pulse in the xy -plane. **c** The envelope of the Bessel pulse in the propagating direction is of a Gaussian type. Here, ω_c is the center frequency of the pulse with center wavelength λ_c . The polar angle of the Bessel pulse is taken as $\theta_c = 0.2\pi$. The other parameters are taken as $m = 2$ and $C_0 = 100$.

the cone with the same frequency $\omega = c|\mathbf{k}|$, k_z , and polar angle $\theta_k = \theta_c$ as shown in Fig. 2a. Then, the SAF of a Bessel pulse with a Gaussian envelope can be expressed $\eta_\lambda(k_z, \rho_k)$ as the product of two Gaussian functions

$$\eta_\lambda(k_z, \rho_k) = \left(\frac{2\sigma_z^2}{\pi}\right)^{1/4} \exp\left[-\sigma_z^2(k_z - k_{z,c})^2\right] \times \left(\frac{2\sigma_\rho^2}{\pi k_{\perp,c}^2}\right)^{1/4} \exp\left[-\sigma_\rho^2(\rho_k - k_{\perp,c})^2\right]. \tag{15}$$

The first Gaussian function with width $1/\sigma_z$ and center wave vector $k_{z,c}$ characterizes the envelope of the pulse in the propagating direction. The pulse length on z -axis in real space is given by $\sigma_z = c\tau_p$ with τ_p the pulse length in time domain (please refer to Supplementary Note 3). We show the energy density of a Bessel pulse in Fig. 2b, c.

Distinct from previous works^{30,50}, we do not add a delta function [such as $\delta(\theta_k - \theta_c)$] in the SAF to characterize its distribution property in the xy -plane. This will cause a serious issue that the wave functions of the quantum pulses cannot be normalized, because $\int d^3k |\xi_\lambda(\mathbf{k})|^2 \propto \delta(\theta_k - \theta_c)$. Instead, we utilize another Gaussian function with width $1/\sigma_\rho$ and center value $k_{\perp,c} = k_{z,c} \tan \theta_c$. These two Gaussian functions should have the same ratio between center wave-number and the width, i.e. $k_{z,c}\sigma_z = k_{\perp,c}\sigma_\rho \equiv C_0$. In the narrow bandwidth limit $C_0 \gg 1$, our defined SAF is well normalized (please refer to Supplementary Note 3). We also note that in contrast to the Bessel-mode-based method³¹ which only applies to Bessel beams, our generalized plane-wave-based framework is amenable to unify the theory of all classes of quantum pulses.

Quantum statistics of the photon spin. Traditionally, the angular momentum carried by each photon in a twisted laser beam has been calculated semi-classically via the ratio of angular flux to the energy flux^{23,24} and only its projection on the propagating axis has been studied. Although the projection of the photon spin and OAM of a non-paraxial beam on the transverse plane has caused attention recently^{25–27,29,34}, a systematic and comprehensive investigation of the vector nature of the photon spin and OAM is still missing. Specifically, the Heisenberg uncertainty relation for photon OAM has never been investigated. On the other hand, many researchers have also tried to establish a quantum theory of the angular momentum of light in the last two decades^{30–33,51}. However, a fully quantum framework to handle arbitrary quantum pulses beyond the paraxial approximation has not been found.

We first calculate the mean value of the spin of a Fock-state Bessel pulse with polarization λ and photon number n (please

refer to Supplementary Note 4),

$$\langle n_{\xi\lambda} | \hat{\mathbf{S}}^{\text{obs}} | n_{\xi\lambda} \rangle = \hbar n \lambda (0, 0, \cos \theta_c). \tag{16}$$

Here, we see that the magnitude of the spin carried by each circularly polarized photon is usually smaller than \hbar and approaches to \hbar asymptotically in the paraxial limit ($\theta_c \rightarrow 0$)^{26,30}.

This is significantly different from the helicity, which is exactly \hbar . If the SAF of a pulse is symmetric in the xy -plane, then the mean value of the spin in the xy -plane vanishes, i.e., $\langle \hat{S}_x^{\text{obs}} \rangle = \langle \hat{S}_y^{\text{obs}} \rangle = 0$. However, we show that the quantum fluctuations of photon spin in the xy -plane are not zero. The standard derivations of the spin of an n -photon Fock-state Bessel pulse are given by

$$\Delta \hat{S}_x^{\text{obs}} = \Delta \hat{S}_y^{\text{obs}} = \hbar \sqrt{n/2} |\sin \theta_c|, \Delta \hat{S}_z^{\text{obs}} = 0. \tag{17}$$

This is significantly beyond the previous semi-classical theory^{23,24,34}, in which the quantum statistics of the photon spin cannot be studied.

Similarly, we can evaluate the mean value of the spin of a coherent-state Bessel pulse with polarization λ and photon number $\bar{n} = |\alpha|^2$,

$$\langle \alpha_{\xi\lambda} | \hat{\mathbf{S}}^{\text{obs}} | \alpha_{\xi\lambda} \rangle = \hbar \bar{n} \lambda (0, 0, \cos \theta_c). \tag{18}$$

Here, we see that the average spin carried by each photon is still $\hbar \cos \theta_c$ and the spin's projection on xy -plane also vanishes. However, the quantum statistics of the photon spin for a coherent-state pulse is significantly different from that of a Fock-state pulse,

$$\Delta \hat{S}_x^{\text{obs}} = \Delta \hat{S}_y^{\text{obs}} = \hbar \sqrt{\bar{n}/2} |\sin \theta_c|, \Delta \hat{S}_z^{\text{obs}} = \bar{n} \hbar |\cos \theta_c|. \tag{19}$$

The Poisson statistics of a coherent pulse leads to non-vanishing $\Delta \hat{S}_z^{\text{obs}}$ in contrast to a sub-Poisson Fock-state pulse.

Quantum statistics of the photon OAM. Heisenberg's uncertainty relation is the canonical quantum characteristics of angular momentum. However, this relation for photon OAM has never been addressed till date. Here, we present a quantitative investigation about the quantum statistics of photon OAM. We discover that for beams with large OAM number, there exist large fluctuations for the OAM operators in the orthogonal directions i.e. in the transverse plane. This quantum effect can be observed in experiment even with traditional OAM laser beams. The mean value of \hat{L}_z^{obs} for a Fock-state twisted pulse with photon number n is given by,

$$\langle n_{\xi\lambda} | \hat{L}_z^{\text{obs}} | n_{\xi\lambda} \rangle = -\frac{i\hbar}{2\pi} \int d^3k \eta_\lambda(\mathbf{k}) e^{-im\varphi_k} \frac{\partial}{\partial \varphi_k} \eta_\lambda(\mathbf{k}) e^{im\varphi_k} \tag{20}$$

$$= mn\hbar. \quad (21)$$

This reduces to the well-known result obtained from the semi-classical method that each twisted photon carries $m\hbar$ OAM^{23,24}.

We see that $\langle \hat{L}_z^{\text{obs}} \rangle$ is independent of the photon polarization. It is only determined by the photon number n and integer m in the helical phase factor $\exp(im\varphi_k)$ if $\eta_\lambda(\mathbf{k})$ is not a function of φ_k . We can also verify that, in this case, the mean value of photon OAM in xy -plane vanishes, i.e., $\langle \hat{L}_x^{\text{obs}} \rangle = \langle \hat{L}_y^{\text{obs}} \rangle = 0$ (please refer to Supplementary Note 4).

The quantum variances of the three components of photon OAM for a Fock-state Bessel pulse are given by

$$(\Delta \hat{L}_z^{\text{obs}})^2 = \langle n_{\xi\lambda} | (\hat{L}_z^{\text{obs}})^2 | n_{\xi\lambda} \rangle - \langle n_{\xi\lambda} | \hat{L}_z^{\text{obs}} | n_{\xi\lambda} \rangle^2 = 0, \quad (22)$$

and

$$\begin{aligned} (\Delta \hat{L}_x^{\text{obs}})^2 &= (\Delta \hat{L}_y^{\text{obs}})^2 \\ &= \frac{1}{2} n \hbar^2 \left[(C_0^2 + \frac{1}{4}) x^2 + (C_0^2 + m^2 + \frac{3}{4}) \frac{1}{x^2} - 1 \right] \end{aligned} \quad (23)$$

$$\geq \frac{1}{2} n \hbar^2 \left[\sqrt{(4C_0^2 + 1) \left(C_0^2 + m^2 + \frac{3}{4} \right) - 1} \right] \gg \frac{1}{2} mn\hbar^2, \quad (24)$$

where $x = \tan \theta_c \in (0, \infty)$ and we have used the inequality relation $a^2x^2 + b^2/x^2 \geq 2|ab|$ and the narrow-band condition $C_0 \gg 1$. This immediately leads to the Heisenberg relation

$$\sqrt{(\Delta \hat{L}_x^{\text{obs}})^2 (\Delta \hat{L}_y^{\text{obs}})^2} > \frac{\hbar}{2} |\langle \hat{L}_z \rangle| = \frac{1}{2} mn\hbar^2. \quad (25)$$

The other two Heisenberg relations for photon OAM are trivial due to the vanishing mean values of \hat{L}_x^{obs} and \hat{L}_y^{obs} . Similar results also hold for a coherent-state twisted pulse, but with non-vanishing $(\Delta \hat{L}_z^{\text{obs}})^2 = \hbar^2 \bar{n} m^2$.

Interesting works have been reported to demonstrate the uncertainty relation between the conjugate variables of angle φ of light and its derivative $\hat{l}_z \equiv -i\hbar\partial/\partial\varphi$ in the first-quantization picture^{52,53}, i.e., $\Delta\varphi\theta\Delta l_z \geq \hbar[1 - 2\pi P(\theta)]/2$. In contrast, our focus is the Heisenberg uncertainty corresponding to the canonical 3D angular commutation relation of photons. On the other hand, we note that for transverse EM fields, {Hamiltonian \hat{H} , momentum \hat{P} , helicity $\hat{\Lambda}$ } has been select as the complete set of commuting observables to specify a photon state usually. Here, we see that a single-photon pulse carrying determinate integer OAM in the propagating direction is not the eigen state of $(\hat{L}^{\text{obs}})^2$.

Our predicted large OAM fluctuations in xy -plane can be verified in experiments (see Fig. 3a). The quantum uncertainties of \hat{L}_x^{obs} and \hat{L}_y^{obs} are linearly proportional to the photon number n in a Bessel pulse as shown in Fig. 3b and proportional to the square of the helical phase index m in Eq. (11) as shown in 3c. From Eq. (23), we see that the OAM fluctuations in the transverse plane are strongly dependent on the polar angle θ_c of a Bessel pulse. There exists a minimum-uncertainty angle due to the inequality $a^2x^2 + b^2/x^2 \geq 2|ab|$ ($x = \tan \theta_c$) in (24) as shown in Fig. 3d. For a optical pulse, the ratio C_0 between its center wave number and its width is usually very large, e.g., $C_0 \approx 188$ for a 50 fs pulse with center wave length $\lambda_c = 500$ nm. In our numerical simulation, we set $C_0 = 100$. We note that these large OAM fluctuations in the transverse plane also exist in traditional OAM laser beams, such as the routinely used Laguerre–Gaussian beams in experiments.

Quantum spin texture of a single-photon pulse. We show that the spin texture of a single-photon pulse can exhibit a very rich and interesting structure in the case beyond the paraxial approximation. The photon spin texture is characterized by the spin density operator

$$\hat{\mathbf{s}}^{\text{obs}}(\mathbf{r}, t) = \varepsilon_0 \hat{\mathbf{E}}_\perp(\mathbf{r}, t) \times \hat{\mathbf{A}}_\perp(\mathbf{r}, t). \quad (26)$$

Similar to the electric or magnetic fields, the spin density can be treated as a vector field and can be measured locally⁴⁴. We emphasize that as a vector, the spin density is neither purely longitudinal or purely transverse in most cases. In the single-mode plane-wave limit, the spin density will be a space-independent constant, i.e., $\nabla \times (\hat{\mathbf{s}}^{\text{obs}}(\mathbf{r}, t)) = \nabla \cdot (\hat{\mathbf{s}}^{\text{obs}}(\mathbf{r}, t)) = 0$.

The mean value of the spin density of a Fock-state Bessel pulse is given (please refer to Supplementary Note 5)

$$\langle n_{\xi\lambda} | \hat{\mathbf{s}}^{\text{obs}}(\mathbf{r}, t) | n_{\xi\lambda} \rangle = \lambda (s_\varphi \mathbf{e}_\varphi + s_z \mathbf{e}_z), \quad (27)$$

where

$$s_z = \frac{n\hbar C_0}{2\pi\sigma_z\sigma_\rho^2} \left\{ [J_{m-\lambda}(k_{\perp,c}\rho)]^2 \cos^4 \frac{\theta_c}{2} - [J_{m+\lambda}(k_{\perp,c}\rho)]^2 \sin^4 \frac{\theta_c}{2} \right\} \exp \left[-\frac{(ct - z \cos \theta_c)^2}{2\sigma_z^2 \cos^2 \theta_c} \right], \quad (28)$$

and

$$s_\varphi = \frac{n\hbar C_0 \sin \theta_c}{2\pi\sigma_z\sigma_\rho^2} \left[\cos^2 \frac{\theta_c}{2} J_m(k_{\perp,c}\rho) J_{m-\lambda}(k_{\perp,c}\rho) + \sin^2 \frac{\theta_c}{2} J_{m+\lambda}(k_{\perp,c}\rho) J_m(k_{\perp,c}\rho) \right] \exp \left[-\frac{(ct - z \cos \theta_c)^2}{2\sigma_z^2 \cos^2 \theta_c} \right], \quad (29)$$

with $\mathbf{r} = \rho \mathbf{e}_\rho + z \mathbf{e}_z$. The spin density of a coherent pulse can be evaluated similarly. Here, we can see the following key characters of the spin density: (i) its projection in the xy -plane is symmetric around z -axis. This causes the corresponding spatial integral to vanish as shown in the previous section, i.e., $\langle \hat{S}_x^{\text{obs}} \rangle = \langle \hat{S}_y^{\text{obs}} \rangle = 0$; (ii) its xy -plane projection is parallel or anti-parallel to the azimuth-angle-dependent unit vector \mathbf{e}_φ and it does not have a radial component. This leads to the helical spin texture as shown in Fig. 4; (iii) its xy -plane projection contains the product of two different Bessel functions. The sign of a Bessel functions flips when crossing its zeros. This leads to the oscillation between clockwise and anti-clockwise structures in the spin texture; (iv) its projection on z is independent on φ . For a small angle θ_c , the term $\sim \cos^4(\theta_c/2)$ dominates. Thus, the sign of s_z is always positive (negative) for LCP (RCP) pulse. This leads to the non-vanishing global spin $\langle \hat{S}_{M,z} \rangle$.

We show the spin texture of an LCP single-photon ($n = 1$) Fock-state Bessel pulse in Fig. 4. Here, we only look at the spin density vector field on the plane $k_z z = ct$, at which the Gaussian functions in Eqs. (28) and (29) reach their maxima. In this case, the space-dependent spin density is only a function of the radius ρ and the azimuthal angle φ contained in \mathbf{e}_φ . For a pulse with small polar angle $\theta_c = 0.1\pi$, almost only a clockwise structure can be observed in panel a. However, for a pulse with a larger polar angle $\theta_c = 0.2\pi$, the oscillation between clockwise and counter-clockwise structure can be observed clearly. This oscillation can only be obtained beyond the scalar-field theory and the paraxial approximation. For higher-order Bessel pulses with $m > 0$, the fine structure of the spin density is significantly different from the $m = 0$ case. The innermost ring changes from clockwise to counter-clockwise as shown in panels c and d. We also note that the Bessel pulse with $m = 1$ is very special (see panel c), because the spin texture has a peak instead of a hole at the center.

In Fig. 5, we show more details of the projection of the spin density vector field on xy -plane and z -axis, respectively. In panel a, we look at the projection of the spin density on xy -plane $s_\varphi \mathbf{e}_\varphi$

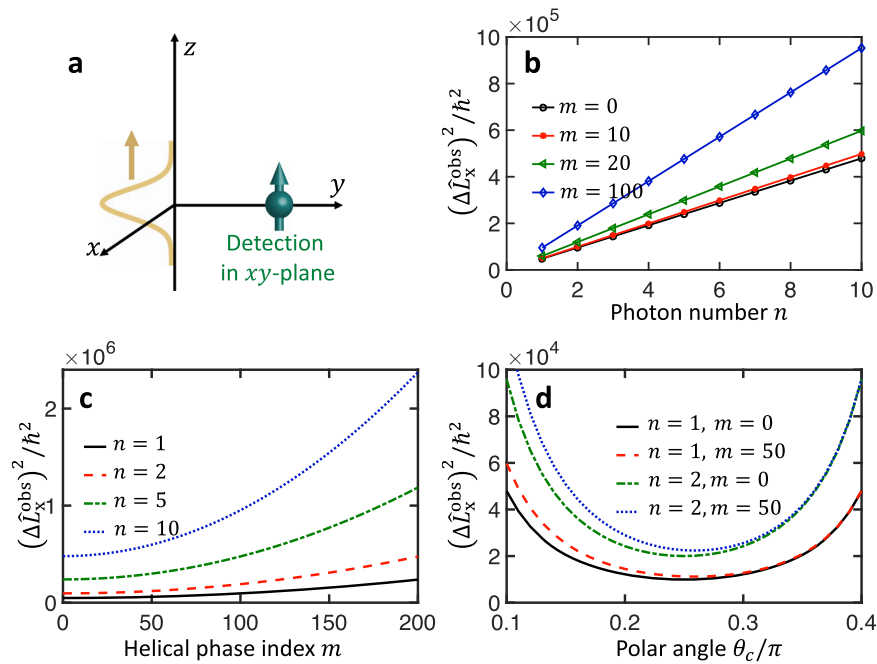


Fig. 3 Photonic orbital angular momentum (OAM) fluctuation in the transverse plane. **a** OAM measurements in the direction orthogonal to the propagating z -axis. A Bessel pulse has vanishing mean OAM in xy -plane but non-zero OAM fluctuations, $(\Delta L_x^{\text{obs}})^2 = (\Delta L_y^{\text{obs}})^2 \iff 0$. **b** The quantum uncertainty of \hat{L}_x^{obs} is linearly proportional to the photon number n in the pulse. Different lines correspond to different helical phase index m . **c** The quantum uncertainty of \hat{L}_x^{obs} is proportional to the square of m . **d** The OAM fluctuation in xy -plane is strongly dependent on the polar angle θ_c of a Bessel pulse. The ratio C_0 has been taken as 100 in all simulations.

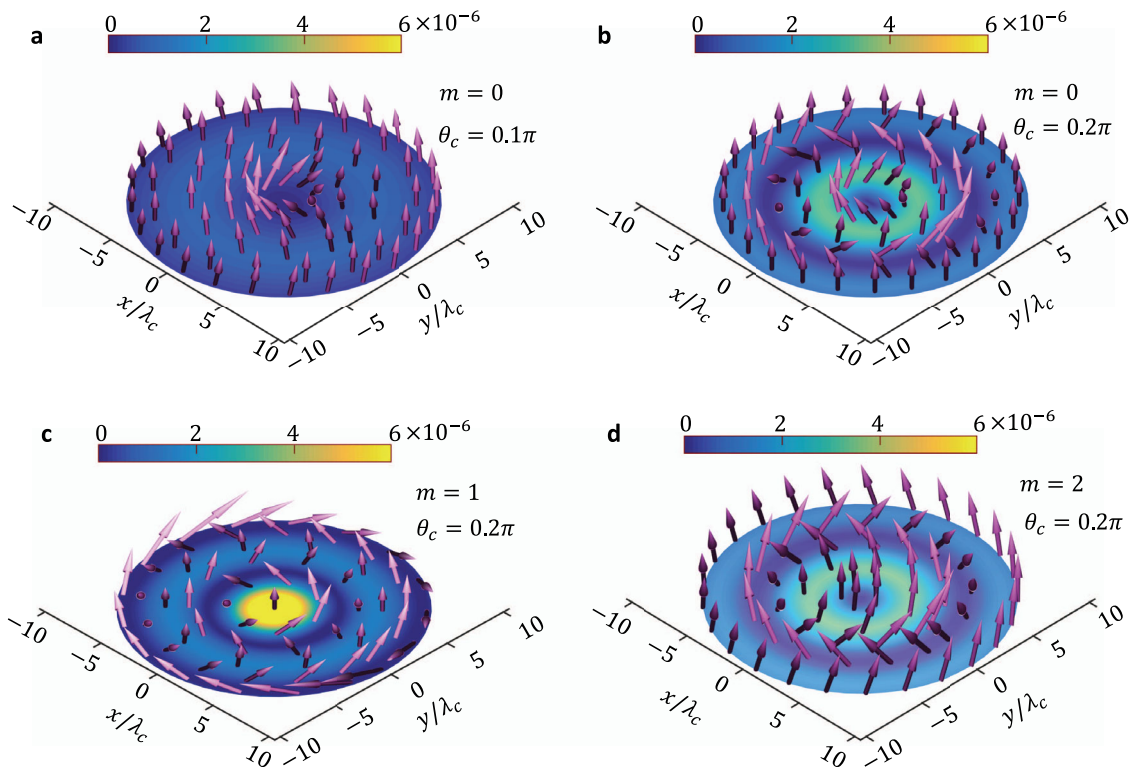


Fig. 4 Helical spin texture of twisted quantum pulse. Spin texture of a single-photon left-circular-polarized Bessel pulse on the pulse-center plane with $k_{z,cz} = ct$. **a–d** Correspond to different quantum numbers m and polar angles θ_c . The colorbar describes the amplitude of spin density in unit of \hbar/λ_c^3 .

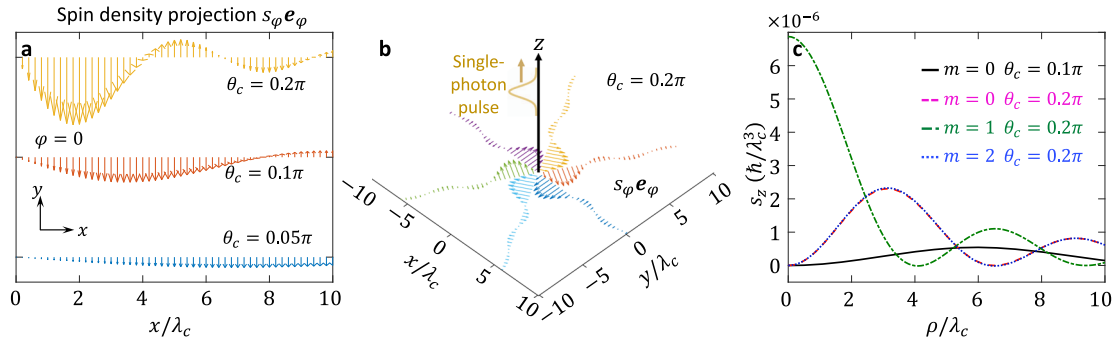


Fig. 5 Details about the spin density vector. Projections of the spin density of a Bessel single-photon pulse on xy -plane (panel **a**, **b**) and on z -axis in panel **(c)**. Panel **a** corresponds to the case with fixed azimuthal angle $\phi = 0$, but different polar angle θ_c . Panel **b** corresponds to the case with fixed polar angle $\theta_c = 0.2\pi$, but different azimuthal angle $\phi = \{0, \pi/3, 2\pi/3, \pi, 4\pi/3, 5\pi/3\}$. Panel **c** shows the z -component of the spin density.

with fixed Bessel order index as $m = 0$ and the azimuthal angle as $\phi = 0$ (i.e., along the x -axis). For a pulse with small θ_c (see the blue arrows at the bottom), $s_\phi e_\phi$ is relatively small and flat. The amplitude of s_ϕ decreases with θ_c and it vanishes when $\theta_c \rightarrow 0$. For a pulse with larger θ_c (see the yellow arrows at the top), the sign of s_ϕ oscillates between ± 1 with increasing ρ . This explains the oscillation between the clockwise and counter-clockwise structures shown in Fig. 4b. In panel **b**, we show the rotation of $s_\phi e_\phi$ in xy -plane with fixed $m = 0$ and $\theta_c = 0.2\pi$. In panel **c**, we show the projection of the spin density on z -axis as the function of ρ for the four cases in Fig. 4. Here, we clearly see the oscillation induced by the Bessel function in Eq. (28). Specifically, the vertex at the center for $m = 1$.

Nonlocal spin noise of light. To characterize the nonlocal spin noise of light, we introduce the quantum correlation function of the photon spin density. Due to the vector nature of the spin density, the full two-point correlation should be characterized by a 3×3 correlation matrix as shown in the Supplementary Note 6. Here, we only describe the equal-time correlator $\langle \hat{s}_z^{\text{obs}}(\mathbf{r}, t) \hat{s}_z^{\text{obs}}(\mathbf{r}', t) \rangle$.

In the paraxial limit ($\theta_c \approx 0$), the two-point correlation functions for a Fock-state and a coherent-state pulse are given by (please refer to Supplementary Note 6)

$$\langle n_{\xi\lambda} | \hat{s}_z^{\text{obs}}(\mathbf{r}, t) \hat{s}_z^{\text{obs}}(\mathbf{r}', t) | n_{\xi\lambda} \rangle \approx \hbar^2 \left[\delta(\mathbf{r} - \mathbf{r}') n |\psi_{-\lambda}(\mathbf{r}, t)|^2 + n(n-1) |\psi_{-\lambda}(\mathbf{r}, t)|^2 |\psi_{-\lambda}(\mathbf{r}', t)|^2 \right], \quad (30)$$

and

$$\langle \alpha_{\xi\lambda} | \hat{s}_z^{\text{obs}}(\mathbf{r}, t) \hat{s}_z^{\text{obs}}(\mathbf{r}', t) | \alpha_{\xi\lambda} \rangle \approx \hbar^2 \left[\delta(\mathbf{r} - \mathbf{r}') \bar{n} |\psi_{-\lambda}(\mathbf{r}, t)|^2 + \bar{n}^2 |\psi_{-\lambda}(\mathbf{r}, t)|^2 |\psi_{-\lambda}(\mathbf{r}', t)|^2 \right], \quad (31)$$

where

$$\psi_\lambda(\mathbf{r}, t) = \frac{1}{\sqrt{(2\pi)^3}} \int d^3 k \xi_\lambda(\mathbf{k}) e^{i[(\mathbf{k}\cdot\mathbf{r} - \omega t) + \lambda\phi_k]}, \quad (32)$$

is the effective wave function of a pulse in real space. This method can be easily generalized to higher-order correlations.

We note that the delta function $\delta(\mathbf{r} - \mathbf{r}')$ in the correlation function will not lead to any diverging effect, because a practical probe always measures the averaged photon spin density over a finite volume instead of the true single-point spin density. On the other hand, this term vanishes in a composite measurement with $\mathbf{r} \neq \mathbf{r}'$. In this case, we see that the Poisson and sub-Poisson statistics automatically enter the quantum spin-density correlations. Specifically, the two-point spin density correlation vanishes for a single-photon Fock-state pulse as expected.

We now propose to detect the non-local spin density correlation via compound measurements of two NV centers, which have been exploited as nano-scale quantum sensors for photonic spin density measurements recently⁴⁴. As shown in Fig. 6a, we fixed one quantum sensor on the z -axis and move the other one to image the distribution of the spin density correlation in the transverse plane. We contrast the spin density correlations in Fock-state and coherent-state Bessel pulses in Fig. 6b–d. Here, we see that in the few-photon limit, there exist significant differences between Fock-state and coherent pulses. This difference fundamentally roots in the quantum statistics of photons and it will disappear in the large-photon limit.

The electronic ground-state of a negatively charged NV center is a spin-1 system, which has been routinely used as a highly sensitive nano-scale magnetometer at room temperature⁵⁴. A laser with wavelength shorter than 637 nm is required to excite the NV to its electronic excited states. A red circularly polarized laser pulse (target pulse) with wavelength around 800 nm will not excite the NV, but only induce energy shifts in the three ground spin states. Recent work has shown that these energy shifts function as a static magnetic field for the NV spin⁴⁴, which is linearly proportional to the local spin density of the target beam, i.e., $\mathbf{B}_{\text{eff}} \propto \langle \hat{s}^{\text{obs}}(\mathbf{r}) \rangle$. Thus, an NV center can be exploited as a nano-scale photonic spin sensor.

Currently, imaging of single-photon level spin density and the corresponding correlation is extremely challenging in experiments. However, our discovered interesting texture of spin density and non-local spin noise also exists in traditional OAM beam, which can be demonstrated in the near future. On the other hand, due to the absence of photon-photon interaction, the nonlocal spin noise within a light pulse in free space is fully determined by the photon-number statistics. However, we predict that exotic photonic phases with long-range spin order can exist in a quantum polariton system or an atomic lattice^{55,56}.

Conclusion

We have established the fully quantum framework for photonic angular momenta of quantum structured pulses, as well as the corresponding quantum texture. Our approach presents a paradigm shift for the photonics community as it can be exploited to study the quantum properties and to reveal the vector nature of the angular momentum of light. We have shown that the spin texture of a Bessel pulse can exhibit a very interesting structure beyond the paraxial limit. Our proposed non-local spin noise will open a frontier for studying exotic phases of photons with long-range spin order. This spin noise can be measured in compound measurements with multiple nano-scale spin sensors, which have been proposed and demonstrated in our previous experiment⁴⁴. The photonic OAM density and the corresponding non-local

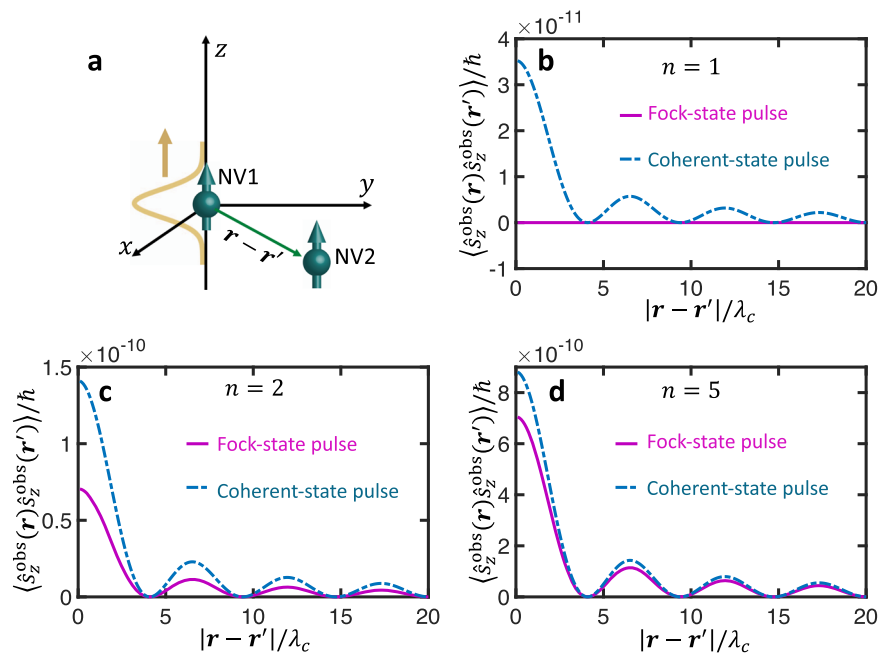


Fig. 6 Non-local spin noise. **a** Our proposed spin density correlation measurement with two nitrogen-vacancy (NV) centers (NV1 and NV2) at \mathbf{r} and \mathbf{r}' , respectively. **b–d** Contrast of spin density correlation between Fock-state and coherent-state pulses. Here, n is the mean photon number in each pulse and we show the results for the case with $m = 1$ and $\theta_c = 0.2\pi$. One of the quantum sensor is fixed on the z -axis and the other sensor can move in xy -plane.

OAM density noise can also be handled within our proposed theoretical framework, which will be addressed in our future work.

Data availability

The data that support this study are available at <https://github.com/yanglp091/PhononicSpinTexture>.

Code availability

The code that supports this study is available at <https://github.com/yanglp091/PhononicSpinTexture>

Received: 8 May 2021; Accepted: 14 September 2021;

Published online: 30 September 2021

References

- Forbes, A., de Oliveira, M. & Dennis, M. R. Structured light. *Nat. Photonics* **15**, 253–262 (2021).
- Forbes, A. & Nape, I. Quantum mechanics with patterns of light: Progress in high dimensional and multidimensional entanglement with structured light. *AVS Quantum Sci.* **1**, 011701 (2019).
- Erhard, M., Fickler, R., Krenn, M. & Zeilinger, A. Twisted photons: new quantum perspectives in high dimensions. *Light: Sci. Appl.* **7**, 17146–17146 (2018).
- Chen, B. et al. Bright solid-state sources for single photons with orbital angular momentum. *Nat. Nanotechnol.* **16**, 302–307 (2021).
- Krenn, M., Handsteiner, J., Fink, M., Fickler, R. & Zeilinger, A. Twisted photon entanglement through turbulent air across Vienna. *Proc. Natl Acad. Sci. USA* **112**, 14197–14201 (2015).
- Zhang, Z. et al. Tunable topological charge vortex microlaser. *Science* **368**, 760–763 (2020).
- Sroor, H. et al. High-purity orbital angular momentum states from a visible metasurface laser. *Nat. Photonics* **14**, 498–503 (2020).
- Ding, D.-S. et al. Quantum storage of orbital angular momentum entanglement in an atomic ensemble. *Phys. Rev. Lett.* **114**, 050502 (2015).
- Zhou, Z.-Q. et al. Quantum storage of three-dimensional orbital-angular-momentum entanglement in a crystal. *Phys. Rev. Lett.* **115**, 070502 (2015).
- Malik, M. et al. Multi-photon entanglement in high dimensions. *Nat. Photonics* **10**, 248–252 (2016).
- Cardano, F. & Marrucci, L. Spin-orbit photonics. *Nat. Photonics* **9**, 776–778 (2015).
- Fang, Y. et al. Photoelectronic mapping of the spin-orbit interaction of intense light fields. *Nat. Photonics* **15**, 115–120 (2021).
- Devlin, R. C., Ambrosio, A., Rubin, N. A., Mueller, J. B. & Capasso, F. Arbitrary spin-to-orbital angular momentum conversion of light. *Science* **358**, 896–901 (2017).
- Stav, T. et al. Quantum entanglement of the spin and orbital angular momentum of photons using metamaterials. *Science* **361**, 1101–1104 (2018).
- Aiello, A., Banzer, P., Neugebauer, M. & Leuchs, G. From transverse angular momentum to photonic wheels. *Nat. Photonics* **9**, 789 (2015).
- Rodríguez-Fortuño, F. J. et al. Near-field interference for the unidirectional excitation of electromagnetic guided modes. *Science* **340**, 328–330 (2013).
- Petersen, J., Volz, J. & Rauschenbeutel, A. Chiral nanophotonic waveguide interface based on spin-orbit interaction of light. *Science* **346**, 67–71 (2014).
- Gong, S.-H., Alpegiani, F., Sciacca, B., Garnett, E. C. & Kuipers, L. Nanoscale chiral valley-photon interface through optical spin-orbit coupling. *Science* **359**, 443–447 (2018).
- Schmiegelow, C. T. et al. Transfer of optical orbital angular momentum to a bound electron. *Nat. Commun.* **7**, 12998 (2016).
- Matula, O., Hayrapetyan, A. G., Fritzsche, S., Surzhykov, A. & Serbo, V. G. Atomic ionization by twisted photons: Angular distribution of emitted electrons. *J. Phys. B At. Mol. Optical Phys.* **46**, 205002 (2013).
- Barik, S. et al. A topological quantum optics interface. *Science* **359**, 666–668 (2018).
- Van Mechelen, T. & Jacob, Z. Viscous Maxwell-Chern-Simons theory for topological electromagnetic phases of matter. *Phys. Rev. B* **102**, 155425 (2020).
- Barnett, S. M. & Allen, L. Orbital angular momentum and nonparaxial light beams. *Opt. Commun.* **110**, 670–678 (1994).
- Berry, M. V. Paraxial beams of spinning light. In *International Conference on Singular Optics*, Vol. 3487, 6–11 (International Society for Optics and Photonics, 1998).
- Monteiro, P. B., Neto, P. A. M. & Nussenzevig, H. M. Angular momentum of focused beams: beyond the paraxial approximation. *Phys. Rev. A* **79**, 033830 (2009).
- Li, C.-F. Spin and orbital angular momentum of a class of nonparaxial light beams having a globally defined polarization. *Phys. Rev. A* **80**, 063814 (2009).
- Cerjan, A. & Cerjan, C. Orbital angular momentum of Laguerre-Gaussian beams beyond the paraxial approximation. *JOSA A* **28**, 2253–2260 (2011).
- Holleccek, A., Aiello, A., Gabriel, C., Marquardt, C. & Leuchs, G. Classical and quantum properties of cylindrically polarized states of light. *Opt. Express* **19**, 9714–9736 (2011).
- Bliokh, K. Y. & Nori, F. Transverse and longitudinal angular momenta of light. *Phys. Rep.* **592**, 1–38 (2015).

30. Arnaut, H. H. & Barbosa, G. A. Orbital and intrinsic angular momentum of single photons and entangled pairs of photons generated by parametric down-conversion. *Phys. Rev. Lett.* **85**, 286–289 (2000).
31. Jáuregui, R. & Hacyan, S. Quantum-mechanical properties of Bessel beams. *Phys. Rev. A* **71**, 033411 (2005).
32. Calvo, G. F., Picón, A. & Bagan, E. Quantum field theory of photons with orbital angular momentum. *Phys. Rev. A* **73**, 013805 (2006).
33. Milione, G., Sztul, H. I., Nolan, D. A. & Alfano, R. R. Higher-order poincaré sphere, stokes parameters, and the angular momentum of light. *Phys. Rev. Lett.* **107**, 053601 (2011).
34. Li, H., Rodríguez-Fajardo, V., Chen, P. & Forbes, A. Spin and orbital angular momentum dynamics in counterpropagating vectorially structured light. *Phys. Rev. A* **102**, 063533 (2020).
35. Loudon, R. *The Quantum Theory of Light* (OUP, 2000).
36. Białynicki-Birula, I. On the wave function of the photon. *Acta Phys. Polonica A* **1**, 97–116 (1994).
37. Sipe, J. E. Photon wave functions. *Phys. Rev. A* **52**, 1875–1883 (1995).
38. Barnett, S. M. Optical Dirac equation. *N. J. Phys.* **16**, 093008 (2014).
39. Yang, L.-P., Khosravi, F. & Jacob, Z. Quantum spin operator of the photon. Preprint at <https://arxiv.org/abs/2004.03771> (2020).
40. Chong, A., Wan, C., Chen, J. & Zhan, Q. Generation of spatiotemporal optical vortices with controllable transverse orbital angular momentum. *Nat. Photonics* **14**, 350–354 (2020).
41. Jhaji, N. et al. Spatiotemporal optical vortices. *Phys. Rev. X* **6**, 031037 (2016).
42. Sachdev, S. *Quantum Phase Transitions* (Wiley Online Library, 2007).
43. Broholm, C. et al. Quantum spin liquids. *Science* **367**, eaay0668 (2020).
44. Kalhor, F., Yang, L.-P., Bauer, L. & Jacob, Z. Quantum sensing of photonic spin density. *Phys. Rev. Res.* Preprint at <https://arxiv.org/abs/2102.11373> (2021).
45. Cohen-Tannoudji, C., Dupont-Roc, J. & Grynberg, G. *Photons and Atoms-Introduction to Quantum Electrodynamics* (Wiley-VCH, 1997).
46. Enk, S. V. & Nienhuis, G. Commutation rules and eigenvalues of spin and orbital angular momentum of radiation fields. *J. Mod. Opt.* **41**, 963–977 (1994).
47. Van Enk, S. & Nienhuis, G. Spin and orbital angular momentum of photons. *EPL (Europhys. Lett.)* **25**, 497 (1994).
48. Romero, G., Ballester, D., Wang, Y. M., Scarani, V. & Solano, E. Ultrafast quantum gates in circuit qed. *Phys. Rev. Lett.* **108**, 120501 (2012).
49. Torres, J. P., Alexandrescu, A. & Torner, L. Quantum spiral bandwidth of entangled two-photon states. *Phys. Rev. A* **68**, 050301 (2003).
50. Jentschura, U. D. & Serbo, V. G. Generation of high-energy photons with large orbital angular momentum by Compton backscattering. *Phys. Rev. Lett.* **106**, 013001 (2011).
51. Babiker, M., Andrews, D. L. & Lembessis, V. E. Atoms in complex twisted light. *J. Opt.* **21**, 013001 (2018).
52. Franke-Arnold, S. et al. Uncertainty principle for angular position and angular momentum. *N. J. Phys.* **6**, 103–103 (2004).
53. Leach, J. et al. Quantum correlations in optical angle–orbital angular momentum variables. *Science* **329**, 662–665 (2010).
54. Barry, J. F. et al. Optical magnetic detection of single-neuron action potentials using quantum defects in diamond. *Proc. Natl Acad. Sci. USA* **113**, 14133–14138 (2016).
55. Asenjo-Garcia, A., Moreno-Cardoner, M., Albrecht, A., Kimble, H. J. & Chang, D. E. Exponential improvement in photon storage fidelities using subradiance and “selective radiance” in atomic arrays. *Phys. Rev. X* **7**, 031024 (2017).
56. Perczel, J. et al. Topological quantum optics in two-dimensional atomic arrays. *Phys. Rev. Lett.* **119**, 023603 (2017).

Acknowledgements

This work is supported by the funding from DARPA Nascent Light–Matter Interactions. L.P.Y. is also supported by the funding from the Ministry of Science and Technology of China (No. 2021YFE0193500).

Author contributions

L.P.Y. and Z.J. conceived the idea and wrote the paper. L.P.Y. performed the calculation under the supervision of Z.J.

Competing interests

The authors declare no competing interests.

Additional information

Supplementary information The online version contains supplementary material available at <https://doi.org/10.1038/s42005-021-00726-w>.

Correspondence and requests for materials should be addressed to Zubin Jacob.

Peer review information *Communications Physics* thanks Jin Liu and the other, anonymous, reviewer(s) for their contribution to the peer review of this work. Peer reviewer reports are available.

Reprints and permission information is available at <http://www.nature.com/reprints>

Publisher's note Springer Nature remains neutral with regard to jurisdictional claims in published maps and institutional affiliations.



Open Access This article is licensed under a Creative Commons Attribution 4.0 International License, which permits use, sharing, adaptation, distribution and reproduction in any medium or format, as long as you give appropriate credit to the original author(s) and the source, provide a link to the Creative Commons license, and indicate if changes were made. The images or other third party material in this article are included in the article's Creative Commons license, unless indicated otherwise in a credit line to the material. If material is not included in the article's Creative Commons license and your intended use is not permitted by statutory regulation or exceeds the permitted use, you will need to obtain permission directly from the copyright holder. To view a copy of this license, visit <http://creativecommons.org/licenses/by/4.0/>.

© The Author(s) 2021